Supplementary information

Ocean surface energy balance allows a constraint on the sensitivity of precipitation to global warming

Wei Wang[1+], TC Chakraborty[2+], Wei Xiao[1], Xuhui Lee[2*]

[1]Yale-NUIST Center on Atmospheric Environment, Nanjing University of Information Science & Technology, Nanjing 210044, China

[2]School of the Environment, Yale University, New Haven, CT 06511, USA.

[+] Authors of equal contribution
[*] Corresponding author: xuhui.lee@yale.edu

Supplementary Figure 1. Ocean surface albedo as a function of global mean 2-m temperature. The annual ocean surface albedo is the ratio of the area-weighted mean outgoing shortwave radiation to the incoming shortwave radiation observed by the Clouds and the Earth's Radiation Energy System (CERES Edition 4.1, https://ceres.larc.nasa.gov/data/). Global mean temperature anomalies are from GISS Surface Temperature Analysis (GISTEMP v4, https://data.giss.nasa.gov/gistemp/). The solid line represents linear regression with the regression statistics noted (N, number of years; R, linear correlation coefficient).

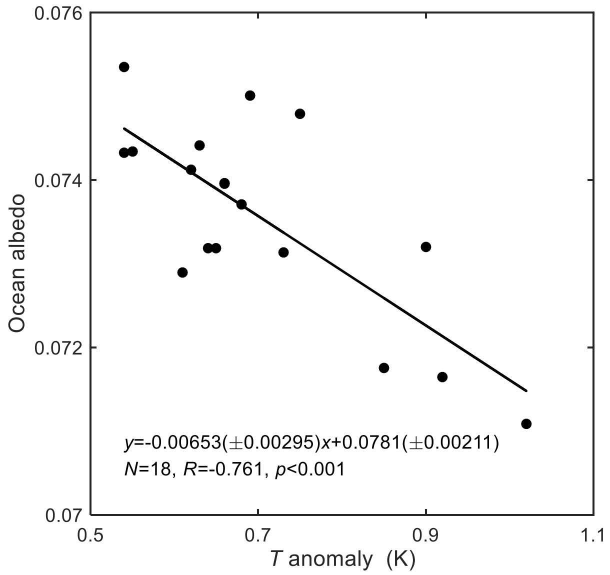

Supplementary Figure 2. Relationship between the land modifier (φ) and tree fraction change. The solid line represents linear regression with the regression statistics noted (N, number of experiments; R, linear correlation coefficient). Error bars are ± one standard deviation. Description of model scenarios is given in Figure 1 caption.

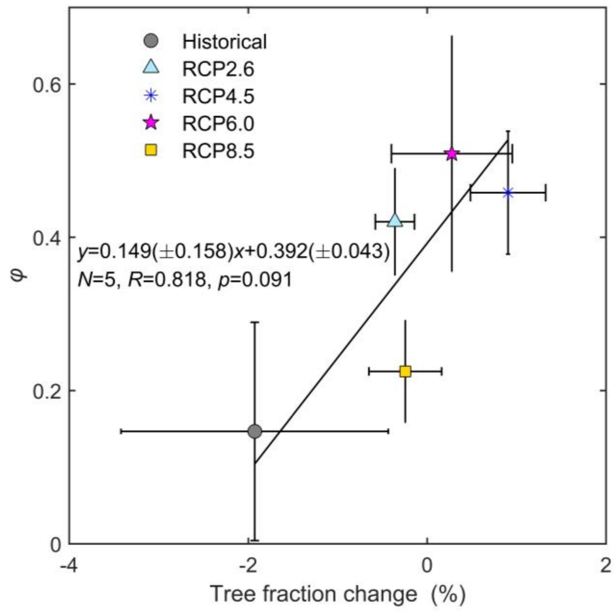

Supplementary Figure 3. Components of the global ocean surface energy balance. The flux is positive in the direction indicated and negative if it goes against the direction shown. a – albedo; β – Bowen ratio; net radiation $R_n = (1-a)K_{\downarrow} + L_{\downarrow} - L_{\uparrow}$.

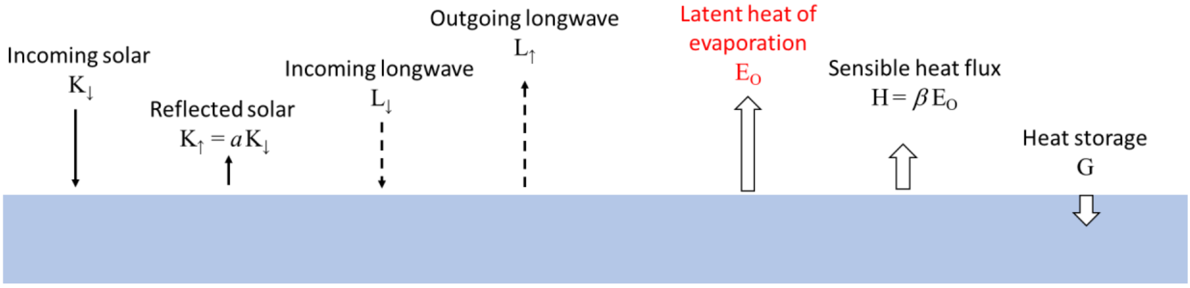

Supplementary Figure 4. Interdependence between temperature sensitivities of incoming shortwave ($\Delta K_{\downarrow}/\Delta T$) and longwave radiation ($\Delta L_{\downarrow}/\Delta T$) at the ocean surface. The solid line represents linear regression with the regression statistics noted (*N*, number of model experiments; *R*, linear correlation). One outlier, marked by light blue filled triangle with the model name noted, is excluded from the statistical calculation. The white circle with error bars (± 1 standard deviation) denotes the observational constraint. The white square denotes sensitivities due to atmospheric moistening under clear skies[1]. Description of model scenarios is given in Figure 1 caption.

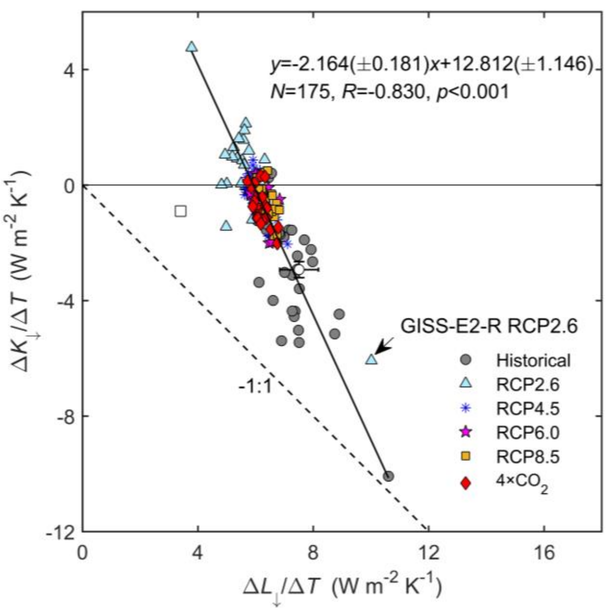

Supplementary Figure 5. Comparison between CMIP5 RCP8.5 and CMIP6 ssp585 scenarios. **a**, Component contributions to global precipitation temperature sensitivity ($\Delta P/\Delta T$). Error bars are ± one standard deviation. **b**, Relationship between changes in global precipitation ΔP and ocean evaporation ΔE_O, with regression statistics indicated (N, number of model experiments; R, linear correlation). **c**, Emergent constraint on global precipitation temperature sensitivity, where the x-axis is the same as in Figure 4a. Solid line represents the regression equation in Figure 4a. Description of model scenarios is given in Figure 1 caption.

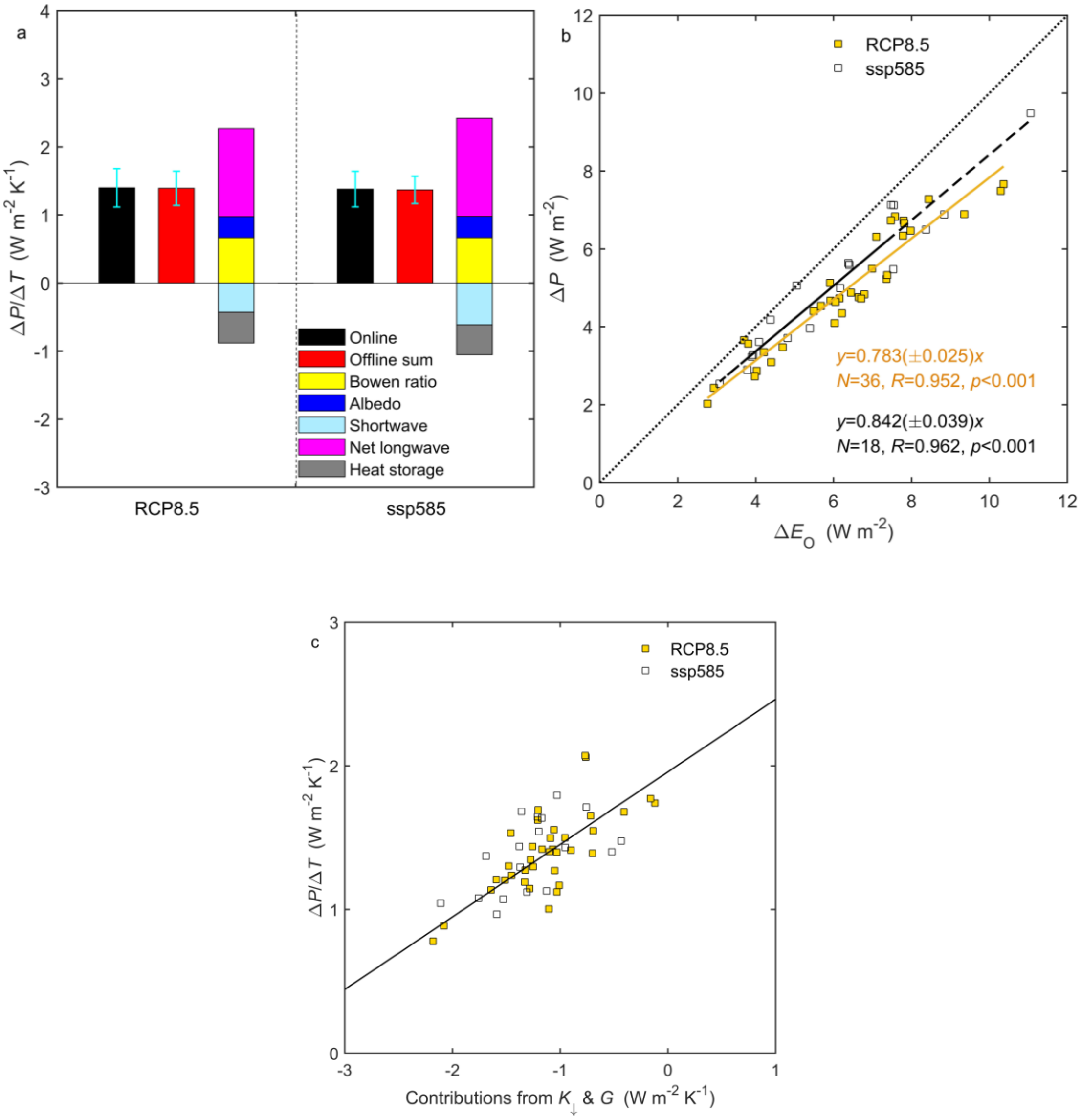

Supplementary Figure 6. Dependence of precipitation temperature sensitivity ($\Delta P/\Delta T$) on feedback strength. Here, the feedback strength α is approximated by the negative value of temperature sensitivity of ocean heat storage ($-\Delta G/\Delta T$) from a $4\times CO_2$ simulation using the same models. The solid lines represent linear regression with the regression statistics noted (R, linear correlation), Description of model scenarios is given in Figure 1 caption.

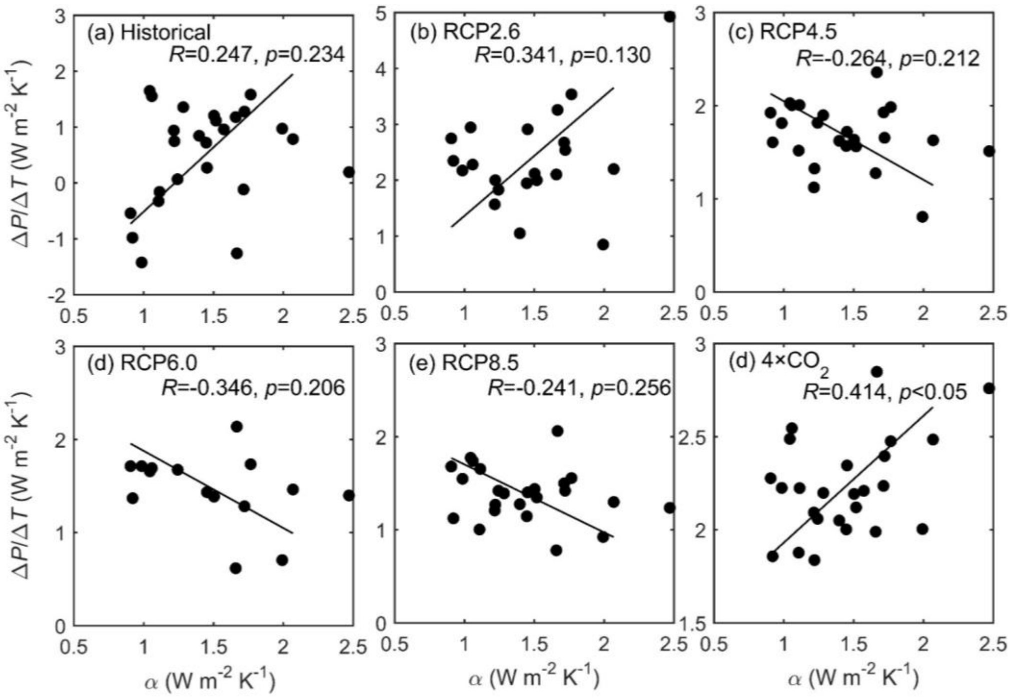

Supplementary Figure 7. Relationship between ocean albedo and ocean incoming shortwave radiation at high latitudes (north of 60° N and south of 60° S). a, annual mean ocean albedo *a* versus annual mean incoming shortwave radiation $K_{\downarrow}$ according to the CERES observation (https://ceres.larc.nasa.gov/data/). **b**, inter-model spread in the *a* and $K_{\downarrow}$ temperature sensitivities for CMIP5 historical simulations. The solid lines represent linear regression with the regression statistics noted (*N*, number of year in panel a and model experiments in panel b; *R*, linear correlation).

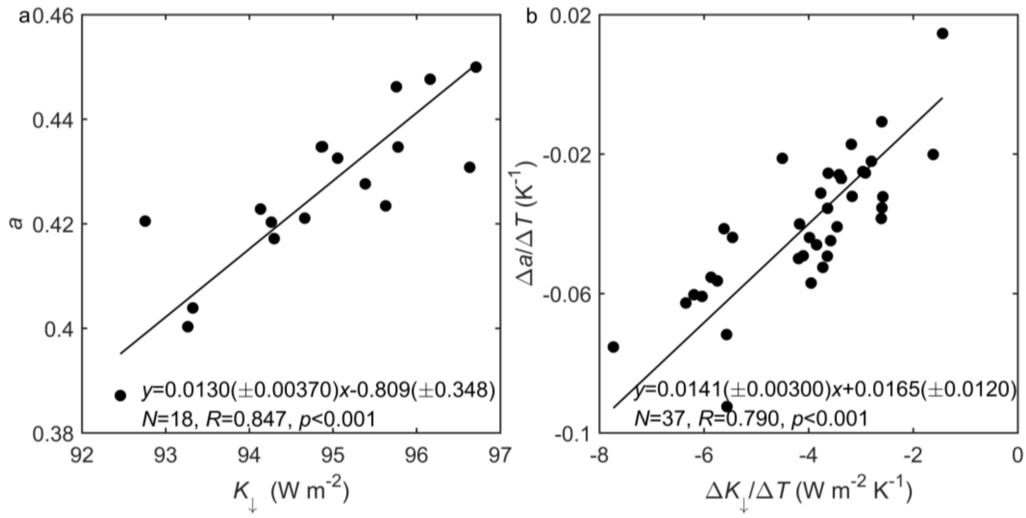

Supplementary Figure 8. Comparison of different definitions of the hydrological climate sensitivity. Data points are annual mean values from the IPSL-CM5A-LR model simulations for three climate scenarios. Solid red circles denote the first and last 10 years of the 4×CO_2 simulation. Red pluses denote the 10-year mean values. In the present study, the slope of *P* versus *T* is approximated by precipitation temperature sensitivity $\Delta P/\Delta T$.

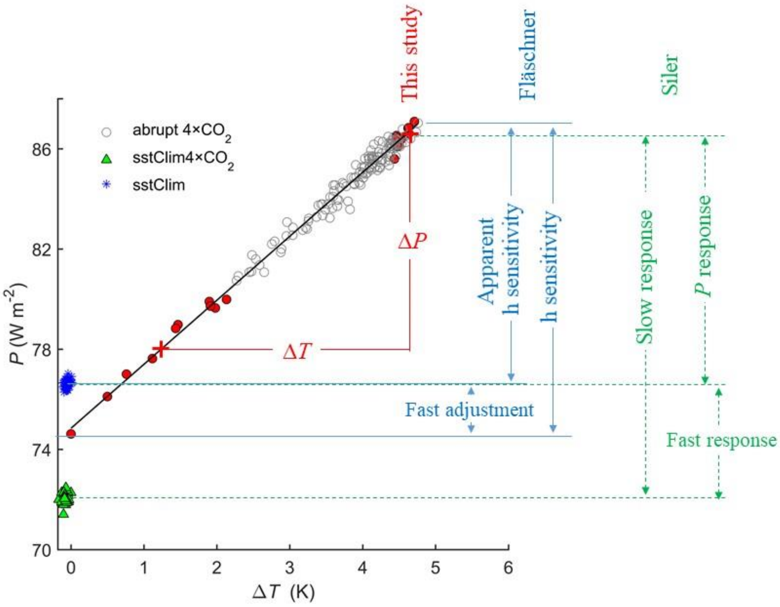

Supplementary Fig. 9. Comparison of regional and global analysis using CMIP5 historical simulations. a, Component contributions to global precipitation temperature sensitivity $\Delta P/\Delta T$ calculated with Equation (1) using global mean values as inputs. **b**, Component contributions from a regional diagnostic analysis, where Equation (1) was applied separately to polar (north 60° N and south of 60° S) and non-polar grids (between 60° N and of 60° S), and the result was weighted by the area fraction of each group to give the global mean value. Red: sum of the five component contributions; yellow: contribution by Bowen ratio change; blue: contribution by surface albedo change; light blue: contribution by change in surface downward shortwave radiation; magenta: contribution by change in surface net longwave radiation; grey: contribution by change in ocean heat storage. Error bars are ± one standard deviation.

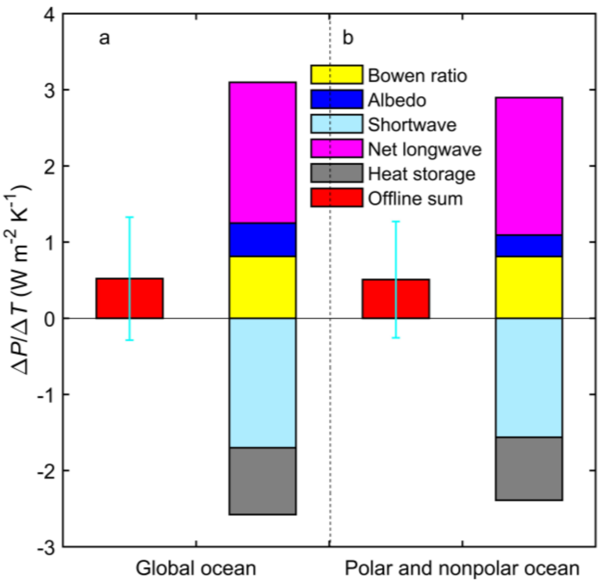

Supplementary Table 1. Regression of changes in global precipitation and in ocean evaporation. For each CMIP scenario, s is the slope of linear regression between changes in global precipitation (ΔP) and ocean evaporation (ΔE_O) across models (with intercept forced through zero), where ΔP and ΔE_O are differences in global precipitation and ocean evaporation, respectively, between the last and the first 10-years of each model simulation. For MERRA-2, s is the slope of linear regression between annual global P and global E_o (with intercept forced through zero). Uncertainty range is ± one standard deviation, estimated as half of the 95% confidence bound on the regression slope. N – number of models (climate scenarios) or number of years (reanalysis); φ − land modifier, the ratio of land evaporation change to ocean evaporation change; R − linear regression coefficient. All correlations are significant at $p < 0.001$.

	N	***s***	***φ***	***R***
Climate model scenario				
CMIP5 Historical	36	0.754±0.054	0.152±0.185	0.987
CMIP5 RCP2.6	25	0.822±0.027	0.385±0.094	0.986
CMIP5 RCP4.5	34	0.821±0.027	0.381±0.093	0.966
CMIP5 RCP6.0	19	0.825±0.047	0.395±0.163	0.946
CMIP5 RCP8.5	37	0.783±0.025	0.253±0.085	0.952
CMIP5 4×CO2	25	0.762±0.013	0.180±0.046	0.984
CMIP6 ssp585	18	0.842±0.039	0.455±0.136	0.962
Reanalysis				
MERRA-2	38	0.695±0.013	-0.051±0.045	0.992

Supplementary Table 2. Empirical constraints on the energy balance components at the ocean surface. Refer to Figure S3 for symbol definitions.

Variable	Mean	S.D.	Reference or data source
Temperature sensitivity			
$\frac{\Delta\beta}{\Delta T}$ (K^{-1})	-0.00834	0.000188	Yang & Roderick (ref. 2)
$\frac{\Delta a}{\Delta T}$ (K^{-1})	-0.00653	0.00147	CERES; Kato et al (ref. 3)
$\frac{\Delta K_{\downarrow}}{\Delta T}$ (W m^{-2} K^{-1})	-2.93	0.276	Reanalysis products
$\frac{\Delta L_{\downarrow}}{\Delta T}$ (W m^{-2} K^{-1})	7.51	0.672	Reanalysis products
$\frac{\Delta L_{\uparrow}}{\Delta T}$ (W m^{-2} K^{-1})	5.24	0.0191	Stefan-Boltzmann Law
$\frac{\Delta G}{\Delta T}$ (W m^{-2} K^{-1})	0.625	0.0257	Cheng et al. (ref. 4)
Ocean energy balance components			
R_n-G (W m^{-2})	116		Wild et al. (ref. 5)
$K_{\downarrow}$ (W m^{-2})	185		
a	0.0811		
β	0.160		

Supplementary Table 3. Sensitivity of incoming surface shortwave $K_\downarrow$ and longwave radiation $L_\downarrow$ to global temperature T. The sensitivity value is calculated as the regression slope of the annual mean $K_\downarrow$ or $L_\downarrow$ over ocean grids against the global mean temperature and adjusted slightly to remove the bias in $K_\downarrow$ or $L_\downarrow$ in reference to the CERES value (https://ceres.larc.nasa.gov/data/). Also shown is the coefficient of determination R^2. All regressions are significant at $p < 0.0001$. The MERRA-2 $\Delta K_\downarrow/\Delta T$ (value in parentheses) is excluded from the mean value given in Supplementary Table 2.

	$\Delta K_\downarrow/\Delta T$		$\Delta L_\downarrow/\Delta T$		
Data source	W m^{-2} K^{-1}	R^2	W m^{-2} K^{-1}	R^2	Period
NOAA-CIRES https://psl.noaa.gov/	-2.36	0.27	6.28	0.92	1851-2014
NCEP-NCAR https://psl.noaa.gov/	-3.43	0.63	8.53	0.96	1948-2019
JRA-55 https://rda.ucar.edu/	-3.55	0.63	6.17	0.95	1958-2013
ERA-5 https://cds.climate.copernicus.eu/	-2.41	0.52	5.54	0.95	1980-2019
MERRA-2 https://esgf-node.llnl.gov/search/create-ip/	(-9.16)	0.52	8.90	0.89	1980-2019

Supplementary Table 4. List of CMIP5 and CMIP6 climate model simulations used in this study. The CMIP5 simulation periods for historical, future (RCP2.6, RCP 4.5, RCP6.0 and RCP8.5) and 4×CO2 scenarios are 1850 - 2005, 2006 - 2100 and 1850 - 1999, respectively. For CMIP6 ssp5-8.5, the simulation period is 2015-2100. Symbol T denotes availability of tree fraction data. Model CMCC-CMS does not output evaporation data and is not used in Fig. 1. BNU-ESM historical experiment is not used for tree fraction analysis presented in Supplementary Fig. 2 because it shows an unrealistically large tree fraction increase in the historical period. Model GISS-E2-R RCP2.6 has an unusually high global precipitation temperature sensitivity. Unless stated otherwise, GISS-E2-R RCP2.6 is excluded from the analysis.

Model name	Historical	RCP2.6	RCP4.5	RCP6.0	RCP8.5	4×CO_2	ssp585
				CMIP5			
ACCESS1.0	Y	N	Y	N	Y	Y	
ACCESS1.3	Y	N	Y	N	Y	Y	
BCC-CSM1.1	Y	Y	Y	Y	Y	Y	
BCC-CSM1.1m	Y	Y	Y	Y	Y	Y	
BNU-ESM	Y, T	Y, T	Y, T	N	Y, T	Y, T	
CCSM4	Y	Y	Y	Y	Y	Y	
CESM1(CAM5)	Y	Y	Y	Y	Y	N	
CMCC-CESM	Y, T	N	N	N	Y, T	N	
CMCC-CM	Y	N	Y	N	Y	N	
CMCC-CMS	Y	N	Y	N	Y	N	
CNRM-CM5	Y	Y	Y	N	Y	Y	
CSIRO-Mk-3-6-0	Y	Y	Y	Y	Y	Y	
CanESM2	Y	Y	Y	N	Y	Y	
FGOALS-g2	Y	Y	Y	N	Y	Y	
GFDL-CM3	Y, T	Y, T	Y, T	Y, T	Y, T	Y, T	
GFDL-ESM2G	Y, T	Y, T	Y, T	Y, T	Y, T	Y, T	
GFDL-ESM2M	Y, T	Y, T	Y, T	Y, T	Y, T	Y, T	
GISS-E2-H	Y	Y	Y	Y	Y	Y	
GISS-E2-H-CC	Y	N	Y	N	Y	N	
GISS-E2-R	Y	Y	Y	Y	Y	Y	
GISS-E2-R-CC	Y	N	Y	N	Y	N	
HadGEM2-CC	Y, T	N	Y, T	N	Y, T	N	
HadGEM2-ES	Y	Y, T	Y, T	Y, T	Y, T	Y, T	
INM-CM4	Y, T	N	Y, T	N	Y, T	N	
IPSL-CM5A-LR	Y, T	Y, T	Y, T	Y, T	Y, T	Y, T	
IPSL-CM5A-MR	Y, T	Y, T	Y, T	Y, T	Y, T	Y, T	
IPSL-CM5B-LR	Y, T	NT	Y, T	N	Y, T	Y, T	
MIROC-ESM	Y, T	Y, T	Y, T	Y, T	Y, T	Y, T	
MIROC-ESM-CHEM	Y, T	Y, T	Y, T	Y, T	Y, T	NT	
MIROC5	Y, T	Y, T	Y, T	Y, T	Y, T	N	

MPI-ESM-LR	Y, T	Y, T	Y, T	N	Y, T	Y, T	
MPI-ESM-MR	Y, T	Y, T	Y, T	N	Y, T	Y, T	
MPI-ESM-P	Y, T	N	N	N	N	Y, T	
MRI-CGCM3	Y	Y	Y	Y	Y	Y	
MRI-ESM1	Y	N	N	N	Y	N	
NorESM1-M	Y	Y	Y	Y	Y	Y	
NorESM1-ME	Y	Y	Y	Y	Y	N	
CMIP6							
AWI-CM-1-1-MR							Y
BCC-CSM2-MR							Y
CAMS-CSM1-0							Y
CanESM5							Y
CESM2							Y
CESM2-WACCM							Y
EC-Earth3							Y
EC-Earth3-Veg							Y
FGOALS-f3-L							Y
FGOALS-g3							Y
GFDL-ESM4							Y
INM-CM4-8							Y
INM-CM5-0							Y
IPSL-CM6A-LR							Y
MIROC6							Y
MPI-ESM1-2-HR							Y
MRI-ESM2-0							Y
NESM3							Y

Supplementary References

1. Pendergrass, A. G. & Hartmann, D. L. The atmospheric energy constraint on global-mean precipitation change. *J. Clim*. **27**, 757–768 (2014).
2. Yang, Y. & Roderick, M. L. Radiation, surface temperature and evaporation over wet surfaces. *Q. J. R. Meteorol. Soc*. **145**, 1118–1129 (2019).
3. Kato, S. et al. Surface irradiances of edition 4.0 clouds and the Earth's radiant energy system (CERES) energy balanced and filled (EBAF) data product. *J. Clim.* **31**, 4501–4527 (2018).
4. Cheng, L. et al. How fast are the oceans warming? *Science* **363**, 128–129 (2019).
5. Wild, M. et al. The energy balance over land and oceans: an assessment based on direct observations and CMIP5 climate models. *Clim. Dynam* **44**, 3393–3429 (2015).